

Automatic Identification of Specular Detections in Multistatic Sonar Systems

Doug J. Grimmer
SPAWAR Systems Center Pacific
53560 Hull Street
San Diego, CA 92152-5000 USA

Abstract- Multistatic systems have the potential to provide increased ASW performance. However, effective fusion and tracking of multistatic active sonar contacts is challenging, due to high levels of false alarm clutter present on all sonar nodes. Such false alarms often overload the sensor-to-fusion-center communications links and fusion/tracking processes, thereby producing too many false tracks. A system concept referred to as Specular-Cued Surveillance Web (SPECSweb) has the potential to solve this overloading problem. This is done through the exploitation of very strong specular echoes from targets operating within a geometrically diverse sensor field. The strong specular echoes are used as cues for track initiation and track holding through selective extraction of additional detections stored locally on the individual sonar nodes. This approach significantly reduces the data rate at the input to the fusion/tracking algorithm, and reduces node-to-fusion-center communication link throughput requirements. A SPECSweb information fusion and target tracking algorithm has been designed, which has shown to be effectively in providing this unloading. Previously, the identification of specular detections was made by simply setting a higher-than-normal SNR detection threshold at the tracker input. This paper presents an alternate approach for detecting specular echoes, which is based on the identification of amplitude changes in the detection levels corresponding to a target passing through the specular geometric condition. The approach is data-adaptive and more robust than the method used previously. The algorithm is described and factors important for parameter value selection are discussed. The proposed identification scheme is applied to multistatic data, showing its effectiveness.

I. INTRODUCTION

Distributed multistatic active sonar networks have the potential to increase ASW performance against small, quiet, threat submarines in the harsh clutter-saturated littoral and deeper ocean environments. This improved performance comes through the expanded geometric diversity of a distributed field of sources and receivers and results in increased probability of detection, area coverage, target tracking, classification, and localization [1].

However, with the increased number of sensors in a multistatic network, come corresponding increases in the data rate, processing, communications requirements, and operator loading. Without an effective fusion of the multistatic data, the benefits of such systems will be unrealizable. Effective, robust, and automated multi-sensor data fusion and tracking algorithms become an essential part of such systems. Much progress has recently been made in this field [2]; however, overloading due to high false alarm rates is still a major issue.

Multistatic fusion algorithms are still challenged to automatically output a sufficiently low false track/alert rate to the operator in these reverberation- and clutter-rich conditions. Communication links may not have the throughput capacity to transfer all of the associated information from the multistatic nodes to a fusion center.

A concept referred to as the “Specular-Cued Surveillance Web (SPECSweb)” is being pursued to address this data rate problem through “specular cueing”, directed data retrieval, retrospective tracking, and novel fusion techniques. A “specular” or “glint” detection can occur within a multistatic network when a sonar source pings while located at an angle astern of the target’s beam aspect ($\pm 90^\circ$ from the bow), at the same time that a receiver is located with equal angle forward of the target’s beam aspect (or vice versa). This occurs when the bistatic aspect angle (bisector of the source and receiver angles) is perpendicular to the target’s heading, as shown in Fig. 1. Such echoes can exhibit an order of magnitude (or more) increase in received level compared to echoes from targets that are not in the specular geometry. When in the specular geometry, there is greatly increased target strength, producing increased echo energy, as indicated by various models and data analyses. SPECSweb exploits specular echoes received within a multistatic network to achieve significant improvements in target detection, classification, and tracking performance.

This approach provides a robust, automated ASW detection and tracking method, resulting in significant reductions in false alarm rates compared to conventional multistatic fusion methods. The SPECSweb application area is ASW surveillance missions, not time-critical tactical ones. The effectiveness of this cueing and fusion method in obtaining high quality tracker output with greatly reduced input/output false alarm rates has been reported [3-6]. Fig. 2 shows an example of SPECSweb tracker performance compared to a traditional tracking approach, where a vast reduction in the false track rate is achieved. Performance comparisons between SPECSweb and other multistatic trackers have also been reported [7-8].

The success of this concept depends not only on an effective information fusion algorithm, but also on the frequency of occurrence of the specular detection cues (and their latency), which initiate the process. Modeling methods have been derived based on simple geometry-based metrics to evaluate multistatic field configurations for occurrence of specular

opportunities. These show that for distributed multistatic fields with sufficient sensor density and rapid enough ping transmission rates, specular echoes can be obtained with low enough latency for area clearance and other surveillance missions [9]. Fig. 3 shows an example of specular condition loci, passage over which provides specular detection opportunities.

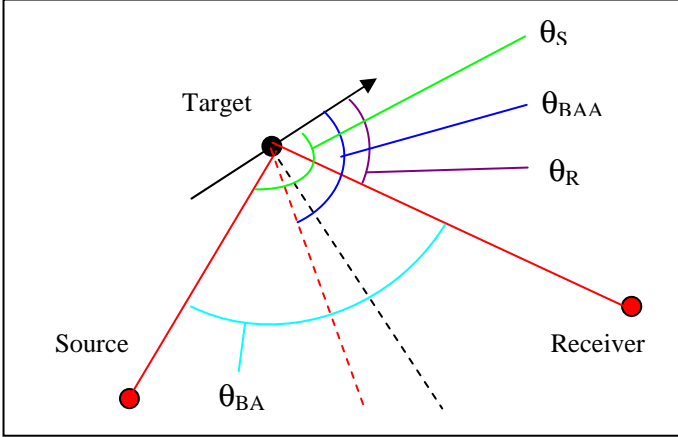


Figure 1. The bistatic geometry; source angle (green), receiver angle (purple), bistatic angle (cyan), bistatic aspect angle (blue), target beam (specular) aspect (black dashed), bisector of source/receiver angles (red dashed). The specular condition occurs when the bistatic aspect angle is $\pm 90^\circ$

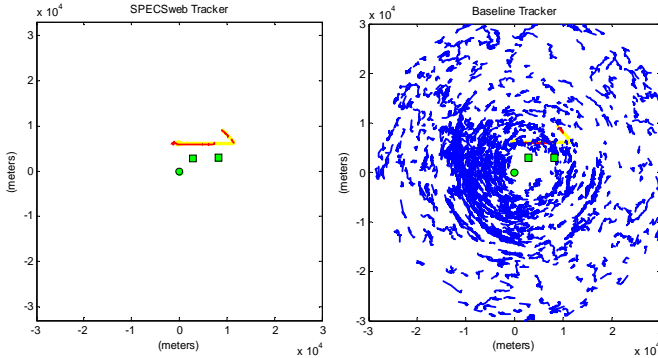


Figure 2. SPECWeb tracker performance (left) versus traditional tracking performance (right) on the same data set; sonar assets (green), target true trajectory (yellow), true tracks (red), false tracks (blue).

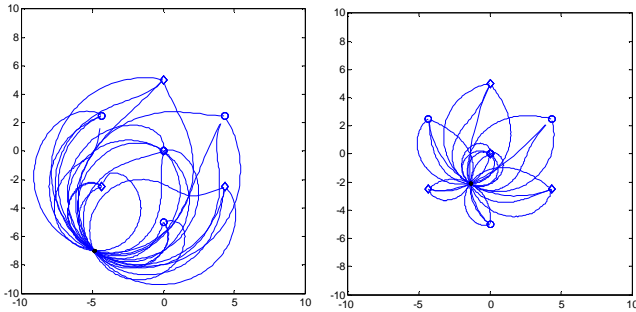


Figure 3. Multistatic field composed of four sources and four receivers, showing specular tripwire loci (blue) for a target: outside the field at $[-5, -7]$ (left), and, inside the field at $[-1, -2]$ (right).

II. SPECSWEB CONCEPT DESCRIPTION

Detailed descriptions of the SPECSweb multistatic tracking algorithm and specular cueing approach are found in [3-4]. A summary of the approach is provided here.

A multistatic scenario consists of multiple, cooperative, fixed or mobile sonar sources and receivers, distributed over an operational area. Sources transmit pulsed signals with different waveform types according to a transmit cycle/schedule. Receivers collect acoustic signals, including target echoes, on arrays of hydrophones. Raw data is band-filtered, beamformed (to provide direction of arrival information), matched filtered (to the transmitted pulse), and normalized. Detection processing is performed to extract and cluster echo energy into detection contacts (true and false). In the SPECSweb concept, the processing is embedded on the receiver nodes, and includes the local storage of all output data. Each receiver packages the contacts corresponding to one source transmission as a single “scan” or “ping” of data.

Multistatic processing provides the following measurements which relate to target kinematics: bistatic time-of-arrival, bearing, and bistatic range-rate (if Doppler-sensitive waveforms are used). Time-of-arrival, bearing, and source/receiver positions are used to calculate the geographic positions (and their uncertainties) of the detections using a non-linear transformation [10].

Each sonar node self-searches each processed (and locally stored) scan for detection contacts which exceed a high SNR threshold setting (HTH). The HTH identifies very strong echoes, which likely correspond to targets that are in the “specular condition”. The HTH normally rejects most (or all) of the false alarm clutter echoes, which have a lower distribution of amplitudes than do specular target echoes (though not necessarily lower levels than non-specular target echoes). Previously, the HTH has been selected using apriori knowledge of target detection performance, however, in real operations, this is difficult to predict (via sonar equation models) with sufficient accuracy. Hence, there is a need for an automatic, data-adaptive identification of specular detections.

Contacts from only FM waveforms which cross the HTH are assumed to be “specular cues”, and only these are initially sent over the communication link to the multistatic fusion center for potential track initiation. By definition, the bistatic specular condition is coincident with targets at zero-Doppler (range-rate). Zero-Doppler echoes from CW waveforms are usually undetectable due to reverberation masking; therefore, only FM waveforms are used as specular cues.

In addition to a target position measurement, a specular cue also provides a target heading measurement. Targets in the specular condition have a heading which is tangential to the bistatic equi-range ellipse at the contact location. There will be an ambiguity between two heading assumptions; one clockwise and one counter-clockwise about the ellipse at this point of tangency. Once a specular cue arrives at the fusion center, two tentative reverse-time tracks are initiated, corresponding to these two headings.

Cues are mapped to x-y positions in Cartesian coordinates, and these positions with their associated error covariances are sent as snippet requests to other nodes. These nodes calculate the appropriate snippet boundaries in their respective measurement spaces within which data association would be possible, according to a specified gating parameter. Any contacts found within the snippet, and above a standard low-threshold (LTH), are sent over the communication links to the fusion center for further processing. As track estimates are obtained, they themselves are used as the cues for selective data retrieval on prior scans stored on any of the nodes. If the retrospective tracking (backtracks) satisfy the initiation criteria, the tracking process continues until a track termination criteria is met. The more likely backtrack is selected, using track-length and heading-stability criteria, and the other backtrack is discarded. Recovering track history in this fashion provides valuable contextual and track classification information. A diagram of the concept is shown in Fig. 4.

The contacts belonging to the selected backtrack are then re-filtered in the forward-time direction, until the current time (of the initiating specular cue) is reached. With this re-filtering, the best possible track estimate at the time of the cue is obtained. At this point the track continues in the forward-time direction updating with measurements found within the retrieval snippets of future scans. Subsequently occurring specular detections update track position and heading, if they are determined to be the nearest neighbor contact in the snippet. New specular detections which are not assignable to existing tracks become new tentative tracks, and the process repeats. Current forward-direction tracks are terminated when the appropriate termination criterion is satisfied.

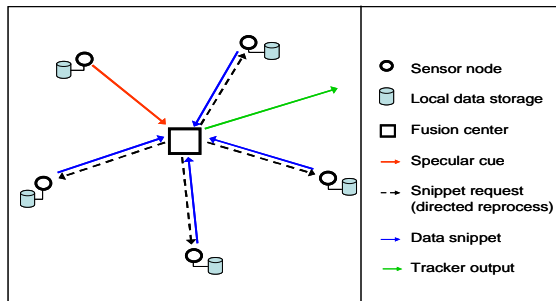


Figure 4. Diagram of the SPECSweb cueing concept.

III. ALTERNATE METHOD FOR SPECULAR DETECTION IDENTIFICATION

Previous SPECSweb fusion/tracking processing has been performed with the analyst choosing optimum settings for a track-initiation threshold level (HTH), knowing a priori the SNR distributions of specular target detections, non-specular target detections, and non-target (clutter) detections for the whole scenario. With such a priori knowledge, track initiation thresholds could be set as high as possible (to remove non-target contacts) while still capturing the specular target

detections. In reality, selection of the (HTH) threshold may not be straightforward. Signal excess predictions (via sonar equation modeling) or other ad-hoc methods for the setting of an absolute track initiation threshold are not viewed as sufficiently robust.

The issues related to setting the HTH are illustrated in Fig. 5, which depicts a contact SNR data series (target in red, background in blue). The background levels are at about the same level as the noise/reverberation background, except in when loud target SNRs are received corresponding to the specular detection. If the HTH is set too high (level A in the figure), the result is disastrous because we fail to obtain a cue and initiate a target track. Setting the HTH to level B is optimum, as it easily rejects all the clutter while detecting the specular echo. However, this level may be difficult to determine a priori. Setting the HTH to level C will cause the SPECSweb tracker to operate more like a traditional tracker, where false alarm (and non-specular target) contacts initiate tracks. Therefore, an automatic method for identification of specular detection cues is preferred.

The proposed alternative method for the automatic identification of specular echoes is not based on the exceedence of an absolute threshold level. Rather, the method is based on evaluating each of the multistatic nodes (source-receiver pairs) for changes in the statistics of their received contact detection levels. Normally, the specular condition will be a very transitory event on a particular node. The specular echo will manifest itself relatively quickly, with a significant positive increase in SNR level from the maximum background levels previously obtained. Rather than calculating a fixed specular threshold, the method is data-adaptive, using current and past data to make a determination of specular detection.

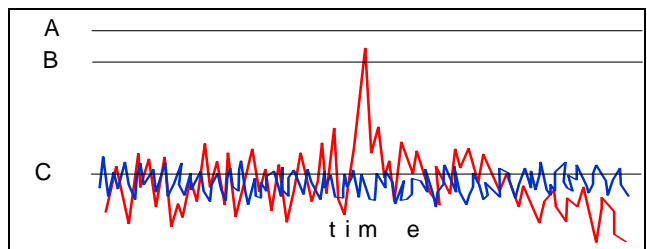


Figure 5. Depiction of the challenge of appropriately setting the SPECSwebs specular (high) threshold (HTH).

IV. BISTATIC TARGET STRENGTH

The objective of this section is to present the bistatic target strength and understand the specular enhancement effect. We characterize the specular effect in terms of its enhancement level and its width. In general, multistatic systems are composed of bistatic sonar nodes, meaning that the source and receiver are not collocated. We therefore consider the bistatic (rather than monostatic) target strength of the target. While the physical structure of a submarine can be quite complex, to first order we can approximate it as a finite cylinder with flat end

caps. The bistatic target strength of such a cylinder is given by [11] as

$$TS = 10 \log_{10} \left[\left(\frac{(2ka) \cdot (L/2)^2 \cdot \sin^2 \theta_s}{\pi (\sin \theta_s + \sin \theta_r)} \right) \times \left(\frac{\sin(kL(\cos \theta_s + \cos \theta_r)/2)}{(kL(\cos \theta_s + \cos \theta_r)/2)} \right)^2 \right], \quad (1)$$

where TS indicates Target Strength (in dB), L is the cylinder length, a is the cylinder radius, k is the wave number ($2\pi f/c$, where f is the sonar frequency and c is the speed of sound), θ_s and θ_r are the angles to the source and receiver, respectively (relative to the target's heading), as seen in Fig. 1. The specular condition occurs when $\theta_s + \theta_r = \pi$, which is where the bistatic aspect angle, θ_{BAA} , is equal to $\pm\pi/2$. The bistatic aspect angle is the angle between the target heading and the bisector of the source/receiver angles.

Fig. 6 shows a plot of the bistatic TS for the case of a receiver at 135° , as a function of source angle, for a frequency of 2250 Hz, length of 55 meters, and radius of 5 meters. Note that the TS reduces significantly for ensonification near the bow and stern, where it is driven by the \sin^2 term. The high-strength specular effect is clearly seen at the specular ensonification angle (in this case, 45°). The lower panel of the plot shows a zoomed view of the specular effect, which is mostly driven by the *sinc* function term in the equation. In this case, the specular effect is seen to be about 15-25 dB above the surrounding lobes of the *sinc* function. As a target moves through the specular condition, it provides increased TS, resulting in an increased detection SNR level and providing the cue needed for SPECSweb tracking. The specular identification method (to be described in more detail later) will watch for the rapid rise in signal level consistent with the specular condition, as received on each of the individual source-receiver nodes over time (pings).

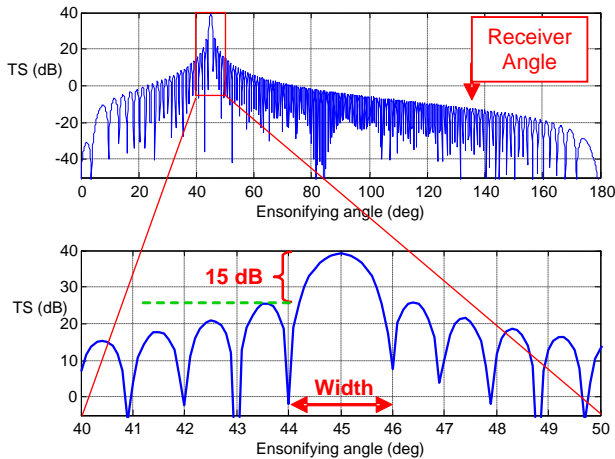


Figure 6. Target Strength of a cylinder as a function of source ensonification angle, for a receiver at 135° , as per equation 1 (top); zoomed view of specular effect (bottom).

The width of the specular peak is important to understand, and it is one of the factors that will dictate how long the enhanced level is available to a source-receiver node. The specular half-width is defined by

$$\beta_{HW} = \frac{\Delta\theta_{null}}{2} = 0.5 \cdot \left\{ \cos^{-1} \left[\frac{2\pi}{kL} - \cos(\pi - \theta_s) \right] - \theta_s \right\}, \quad (2)$$

where $\Delta\theta_{null}$ is the angle from the specular peak to the first null of the *sinc* function, which is the part of the function corresponding to a rise (or fall) in the TS. The 1st null of the *sinc* function occurs when its argument is equal to π . Dividing by two expresses the specular half-width in terms of the bistatic aspect angle (the bistatic aspect angle varies at half the rate as a change in either source or receiver angle alone). The bistatic aspect angle is a more convenient quantity to use in the study of the specular effect.

Using equation 2, the specular half-width (in degrees) is plotted in Fig. 7, as a function of ensonification angle. We assume that the receiver is always positioned in a location needed for the specular condition. In this case, the specular half-width is about 0.4° , except at bow/stern, where it increases dramatically. Bow/stern geometries are not normally useful however, due to the direct-blast blanking effect. Direct-blast blanking occurs when the target is located near the line connecting the source and receiver. In this case, the target echo arrives at the receiver about the same time as the source's direct ping energy, and is therefore often masked and undetectable. The effect of cylinder length and frequency are shown in Fig. 8. The half-width is shown as a function of the bistatic angle, θ_{BAA} (angle between source and receiver, from the target). The specular half-width decreases with increasing target length and frequency of operation. If a more complicated target strength model is deemed appropriate, the specular half-width can be determined in a manner similar to that shown previously.

Consider Fig. 9, which shows six example target trajectories within the surveillance area of a single, fixed bistatic sonar node. The receiver is located at (7.5,0) km and the source is located at (7.5,0) km. An equi-range ellipse is also shown, with targets 1-3 shown in the specular condition (indicated by the red dots) and tangent to the ellipse. Targets 5-6 never encounter a specular condition. Target 4 passes through specular, but at a closer bistatic range than target 3.

In Fig. 10, the trajectories are overlaid on an image of bistatic TS produced by the BASIS target strength model [12]. The BASIS model approximates the target as an assembly of simple component shapes. The TS is obtained by assuming hard boundaries and coherently combining the (analytically) obtained scattering from each component shape. The modeled output is for a frequency of 2250 Hz, radius of 5 meters, a hull section of 55 meters, a conical tail section of 20 meter length, and is plotted by the color scale as a function of bistatic angle and bistatic aspect angle. The specular enhancement is shown as the vertical red line at 90° bistatic aspect angle. The second

enhancement seen at 100° is caused by the modeled submarine's conical tail section. The overlaid trajectories for targets 1-4 traverse the specular enhanced energy peak with different rates. Targets 5 and 6 don't cross the specular energy, with target 5 clearly within the direct blast blanking region. Fig. 11 shows the BASIS target strength for the monostatic case (bistatic angle equal to zero). Here we see that the conical tail section feature is lower than the specular by about 10 dB. The zoomed view shows that the specular half-width is about 0.4 degrees, a value consistent with the cylinder case calculated previously.

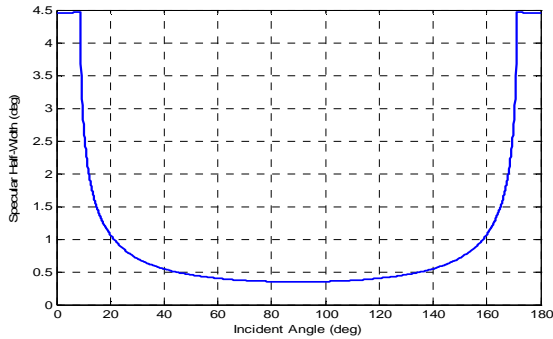


Figure 7. Specular half-width as a function of ensonification angle.

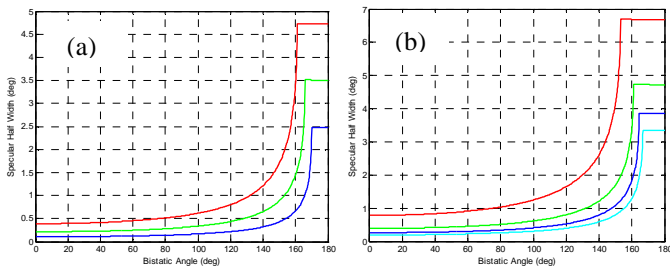


Figure 8. Specular half-width as a function of: (a) target length ($f=2$ kHz), $L=55$ m (red), $L=100$ m (green), $L=200$ m (blue); (b) frequency ($L=55$ m), $f=1$ kHz (red), $f=2$ kHz (green), $f=3$ kHz (blue), $f=4$ kHz (cyan).

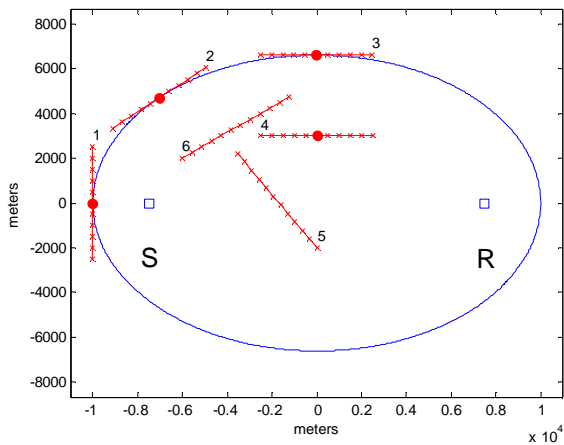


Figure 9. Target trajectories near a bistatic sonar; red dots indicate points of specularity.

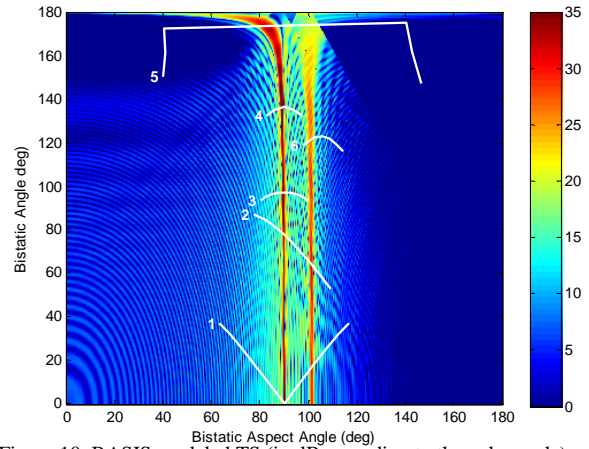


Figure 10. BASIS modeled TS (in dB according to the color scale), as a function of bistatic angle and bistatic aspect angle; trajectories from Fig. 9 are overlaid.

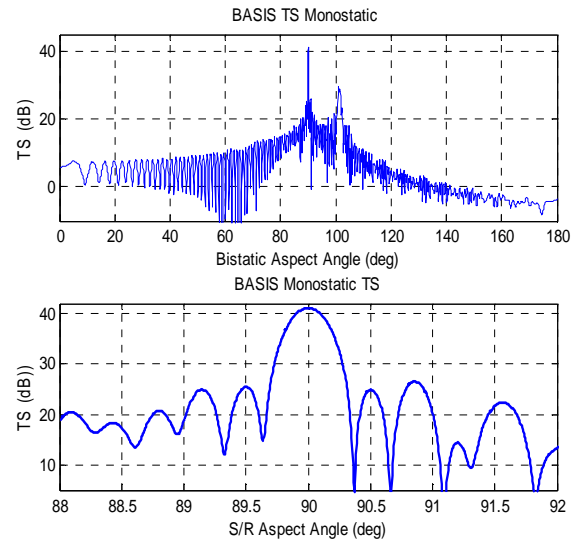


Figure 11. BASIS modeled TS for the monostatic geometry (top); zoomed view of the specular part of target strength (bottom).

V. BISTATIC ASPECT RATE

The example given in the previous section shows that not only is it important to consider the specular width, we must also understand the rate at which a potential target will pass through the specular condition. As the rate at which the target moves through the condition increases, then the probability of obtaining enhanced specular energy in an echo reduces (for a given ping repetition interval). The “bistatic aspect rate” provides a way to measure this effect. This quantity has been derived previously [9] for fixed sources and receivers; here we provide a generalization for the case of mobile assets. The bistatic aspect rate (AR) is the derivative of the bistatic aspect angle with respect to time, and is derived as:

$$AR = \frac{d\theta_{TB}}{dt} = \frac{d(H_T - 0.5 \cdot (\theta_S + \theta_R))}{dt} =$$

$$\begin{aligned} & -0.5 \cdot \frac{(x_S - x_T)(s_S \cdot \sin H_S - s_T \cdot \sin H_T) - (y_S - y_T)(s_S \cdot \cos H_S - s_T \cdot \cos H_T)}{\left[1 + \left(\frac{y_S - y_T}{x_S - x_T}\right)^2\right] \cdot (x_S - x_T)^2} \\ & -0.5 \cdot \frac{(x_R - x_T)(s_R \cdot \sin H_R - s_T \cdot \sin H_T) - (y_R - y_T)(s_R \cdot \cos H_R - s_T \cdot \cos H_T)}{\left[1 + \left(\frac{y_R - y_T}{x_R - x_T}\right)^2\right] \cdot (x_R - x_T)^2} \end{aligned} \quad (3)$$

where $x_S, x_R, x_T, y_S, y_R, y_T$, are the x and y positions, s_S, s_R, s_T , are the speeds, and H_S, H_R, H_T are the headings of the source, receiver, and target, respectively. Thus, given the specular half-width and the position and velocity estimates of the sonar assets and target, we can determine how long (in time, or over what travel distance) specular energy will be available to the bistatic sonar node. The aspect rate (normalized by target speed) is shown for the previous example in Fig. 12. We see an increase in aspect rate when the target is close to the source or receiver. Fig. 13 shows a histogram of the aspect rates in the surveillance box. There is a peak in the distribution around 4 degrees/km. The aspect rate as a function of time can be obtained by multiplying by the hypothesized target speed.

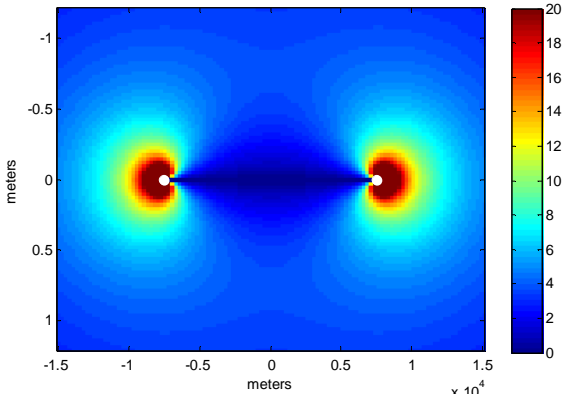


Figure 12. Aspect rate (in degrees/km according to the color scale) for specular targets, as a function of location, relative to the bistatic node of Fig. 10.

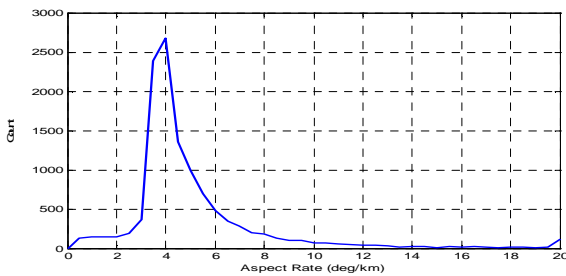


Figure 13. Histogram of Aspect Rate, for the locations in Fig. 12.

VI. DESCRIPTION OF THE ALGORITHM FOR IDENTIFICATION OF SPECULAR DETECTIONS

With the insight gained into the expected strength/width of the specular energy and the expected rate of aspect angle changes (for hypothesized target speeds), we now describe a data-adaptive method to automatically identify specular detections. For specular detection identification, each source-receiver pair (node) is evaluated separately and independently from the others. This is because at any given time, the rise in signal levels (due to the specular enhancement) will only apply to the particular pair that is in the specular geometry. Also, each pair may have its own unique background statistics.

Each source transmission produces a scan of measurements on any given receiver. Only scans from Doppler-insensitive (FM) waveforms are considered for cue identification. Such a measurement scan is illustrated in Fig. 14, which may contain many detection contacts, each with measurements of arrival angle, arrival time, received level (LVL), SNR, as well as other feature or classification information. The scan may be (optionally) divided into segments, as shown in the figure. Note that the early arrival times corresponding to the direct blast region are ignored. Within each segment, the maximum SNR (or, LVL) of all the detection contacts is extracted and stored (indicated by the red colored contacts).

The aforementioned process repeats for each successive measurement scan (and segment), contributing to a maximal data series. There will be a maximal data series maintained and updated for each segment of each source-receiver pair. Fig. 15 shows a depiction of such a maximal data series, which can be monitored for significant changes (i.e., increasing levels) corresponding to received specular energy. Whereas previously a single parameter (HTH) was used, here, two parameters are specified to identify a specular detection: Rise Threshold (RTH, in dB) and Integration Time (IT). A specular detection is identified and declared when the current value of the maximal data series exceeds any previous values within the IT by more than the RTH.

A value for the RTH parameter can be determined by evaluating the specular enhancement in the assumed target strength. For the models discussed in section IV, the specular enhancement was 15-20 dB above non-specular target strength. A more conservative value of ~10 dB may be appropriate choice for RTH in this case, since the absolute peak may not be obtained at the exact time of the ping transmission.

It is also important to understand the effect for maximum-picking on the (false alarm clutter) background statistics. Given the maximal data series expressed by

$$m_N(z_i) = \text{Max}\{z_i, z_{i+1}, z_{i+2}, \dots, z_{i+N-1}\} \quad (4)$$

which takes the maximum of N values of z_i , the cumulative distribution function of the maximal function is the original data's cumulative distribution function raised to the power of N, as

$$F_N(m) = F(F_Z)^N \quad (5)$$

Using this relationship, we can determine the false alarm probability of a maximal data series. Fig. 16 shows the effect of the max-picking process on false alarm probability (log scale) as a function of threshold, at the normalized, detector output, assuming a Rayleigh distributed noise background. A Rayleigh distribution at the output of the matched filter corresponds to a Chi-squared distribution (with 2 degrees of freedom) at the normalized, detector output. It is seen that the false alarm rate increases by about 1 order of magnitude (at thresholds around 12-15 dB) for maximum picking taken over 10 times the number of original samples. In this case, performing maximum picking (over up to 1000 values) requires that the threshold be raised only a couple of dB to maintain same false alarm rate. It is assumed here that the specular effect is observable above this increased max-picked background estimate. In real ocean environments, the background is known to be non-Rayleigh; the actual distributions are heavier-tailed, which would further increase the maximal level of the background.

The IT parameter will control the duration over which to search for specular level changes. A value (or a range of values) for the IT can be determined using by dividing the specular half-width by the aspect rate, as follows:

$$IT = \frac{\beta_{HW}}{AR} \quad (6)$$

The specular half-width may be determined according to the methods described previously. The aspect rate depends on the target location and velocity, which are unknown apriori, but assuming possible ranges of values for the surveillance area will aid in selecting reasonable parameter values.

The first occurring specular cue on a particular node is the one to initiate a target track. Subsequently identified target cues are associated to the existing track if it has been continuously held, rather than initiating a new track. Though the auto-adaptive identification method takes two parameters (vs. one), their settings are more easily determined without apriori information, or relying on imprecise predictive modeling. Reasonable settings of these parameters provide more robust performance than the single HTH used previously.

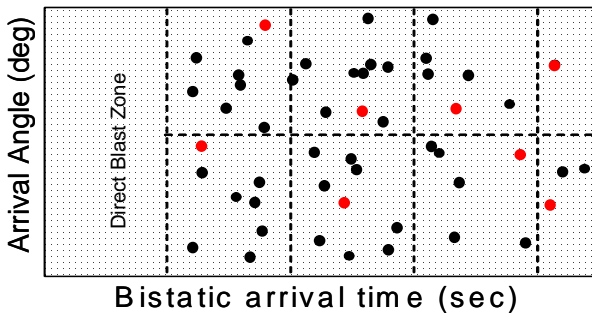


Figure 14. Illustration of a single source-receiver pair's measurement scan, divided into analysis segments. Contacts are shown, with red contacts indicating the contact with the maximum SNR/LVL within each segment.

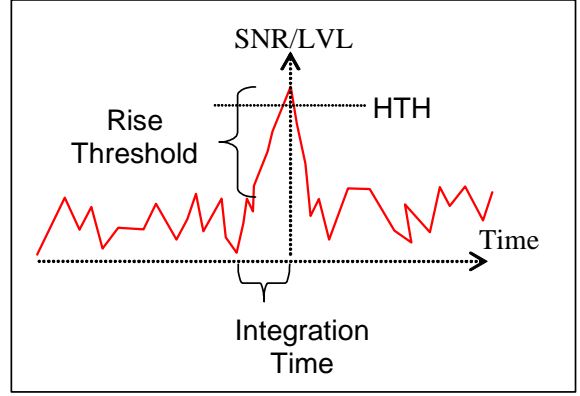


Figure 15. Depiction of a maximal data series analyzed for specular detection.

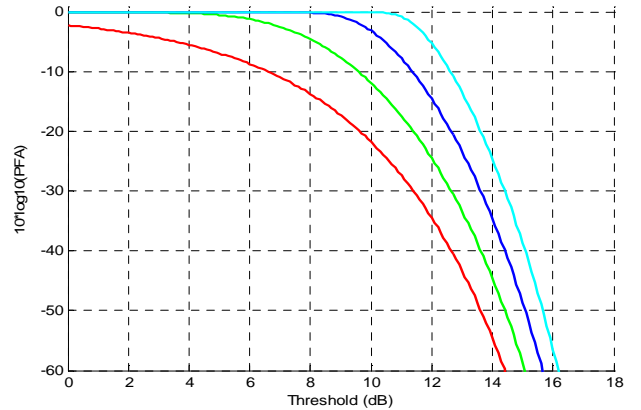


Figure 16. Probability of false alarm for maximal data series (max of N) derived from a Rayleigh distribution; N=1 (red), N=10 (green), N=100 (blue), N=1000 (cyan).

VII. ALGORITHM APPLICATION TO DATASETS

In this section we apply the automatic identification algorithm to simulated and real data, and evaluate its performance.

A. NURC MSTWG Data Set

The Multistatic Tracking Working Group (MSTWG) has provided several multistatic simulated data sets for data fusion and tracking algorithm evaluation [2]. The NATO Undersea Research Center (NURC) has provided a simulated scenario with two sources and two receivers (4 nodes) and an aspect-dependent target with specular detections. A detailed description of this scenario and SPECSweb tracking results can be found in [4,13]. Fig. 17a shows a maximal data series obtained for node #4 of the data set. In this scenario, pings were transmitted every minute for three hours and each scan contained ~200 detection contacts. Every fourth scan corresponds to node #4. In this case the entire measurement scan (60 seconds and 360 degrees) was used to derive the maximal data series (no segmentation was performed, but the direct blast region was ignored). The maximum-picked clutter background is seen to be about 15 dB, a level consistent with the Rayleigh assumption previously analyzed. Other target-related contacts are seen to rise above this level. The specular

detection is seen around scan #272. Using a RTH of 10 dB and an IT of 3 minutes, the automatic identification yielded 4 specular cues, as indicated in the figure by the red markers. Fig. 17b shows the power difference (in dB) between the current scan and the previous scan, with the RTH (of 10 dB) indicated by the red line. One scan (#272) exceeds the threshold in a single (one minute) update. Fig. 17c shows the difference series summed over the previous three minutes (corresponding to the selected IT). Now there are four crossings of the RTH corresponding to the four cues identified (scans 260, 272, 276, and 330). The first three cues are associated with the target's specular effect, and the fourth is the result of a strong non-specular target-originated detection.

Fig. 18 shows the results for all four of the sonar nodes of this scenario. In each case, the blue x's indicates the extracted maximal values, red circles indicate identified cues, and the green dots represent the SNRs of the target. Sometimes the target-originated contacts are the maximal values extracted (when the target SNR and the maximal value are seen to be coincident). This is true during the specular enhancement, as expected, but also during some non-specular periods. The identification algorithm's performance is quite good. It correctly identified the specular target cues on nodes 2-4, without any false cues. Five non-specular target cues are identified on node 1, triggered by significant target SNRs, and without any false cues. Though these cues are not associated with the specular effect, they may still be exploited, with a modification to the SPECSweb tracking algorithm. The SPECSweb tracker may be extended to initiate a 3rd tentative backtrack without an initial (specular) heading assumption.

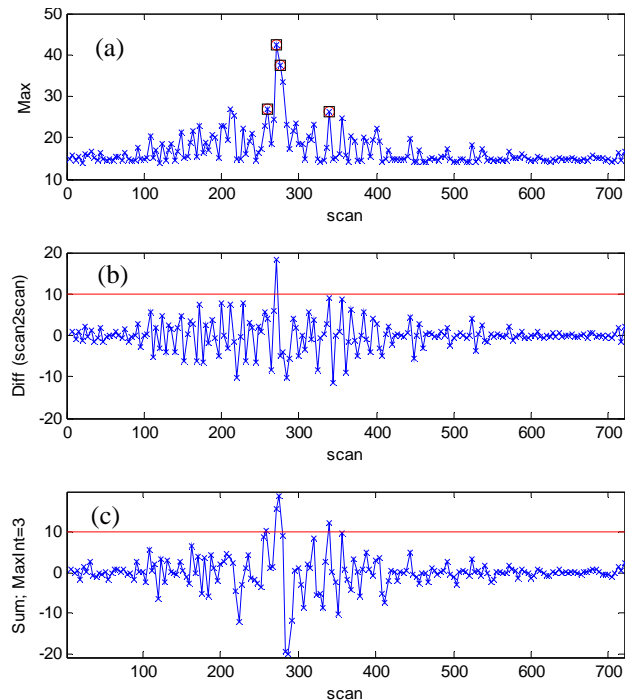


Figure 17. Data from NURC MSTWG Scenario, Node #4; (a) maximal data series over the scenario duration with identified specular detections in red, (b) difference series of Fig. 17a, (c) integration of Fig. 17b over 3 minutes.

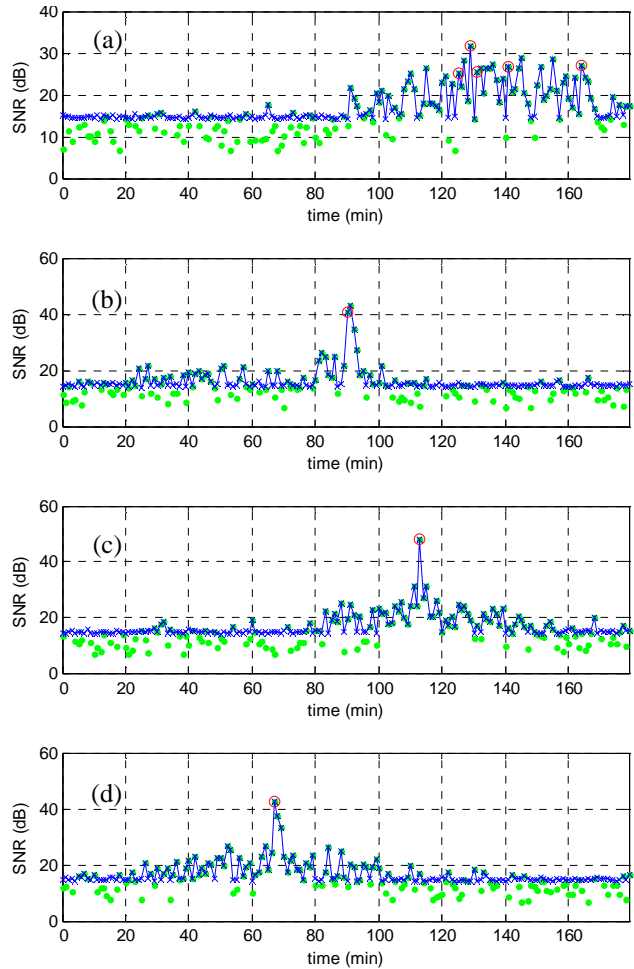


Figure 18. Data from NURC MSTWG Scenario; extracted maximum values (blue); identified cues (red); target-originated contact SNRs (green); (a) node 1, (b) node 2, (c) node 3, (d) node 4.

Fig. 19 shows an evaluation of the identification algorithm's parameters. In Fig. 19a, we see that as the RTH is lowered, we generate larger numbers of cues, as expected. Presumably some of these are triggered on fluctuations of the background noise and can be considered false cues. Others may be triggered by loud non-specular target detections, and can be considered non-specular target cues. In this case, RTHs over the range of 8-18 dB gave good performance for the specular cue identification. The algorithm could not identify all the specular detection cues when the RTH was raised above 18 dB.

Fig. 19b shows the effect of the variation of the IT. With increased integration time, the number of identified cues increases. This is because in this case, there are extended periods with gradual increases in the target contact levels. For this scenario, the specular effect is seen to be quite abrupt, therefore, a shorter integration time is more effective.

The possibility of performing the cue identification within multiple scan segments was previously mentioned. The motivation for segmenting the scans is to allow for the separation of target echoes from other, stronger, consistently occurring echoes corresponding to false targets (like wrecks,

bottom outcrops, etc.). This will allow them to be detected when sufficiently separated (in measurement space). In addition, it allows for multiple targets to be detected by the same node on the same scan, if required. Fig. 19c and 19d show the effect of segmentation size. As more segments are used (smaller segment size), the number of identified cues slightly increases. This is because there are more opportunities to search for cues, as well as the possibility of target contacts moving (over time) from within a particular segment to an adjacent segment. Strong target-originated contacts above the maximal contact background level will likely cause a new identification when shifting into a neighboring segment.

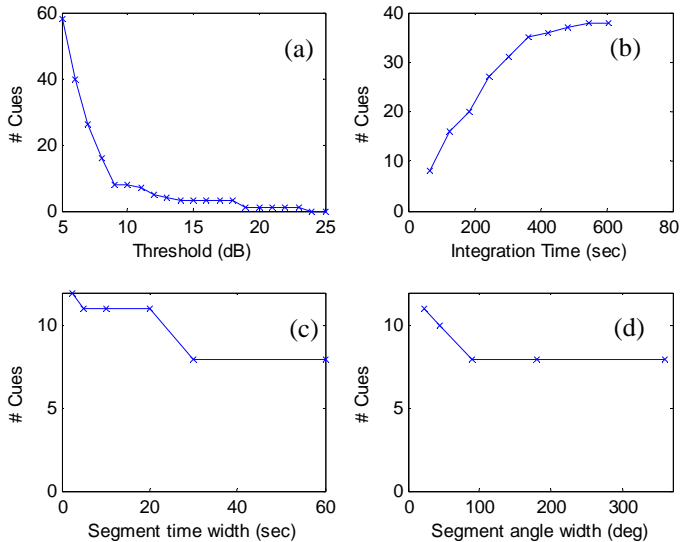


Figure 19. Parameter evaluation; number of cues identified as a function of: (a) RTH, (b) IT, (c) Segment time width, (d) Segment angle width.

B. SEABAR'07 Data Set

The SEABAR'07 sea trial [14] was a multistatic experiment conducted by the NATO Undersea Research Centre (NURC) in the Malta Plateau, south of Sicily, 10-22 October, 2007. The experiment was situated in a challenging shallow water (100-150 meters depths) area, with high levels of reverberation, clutter, and shipping noise. More details of this experiment and SPECSweb tracking results can be found in [3,14]. For this paper, run A56 (duration 140 minutes) of the experiment was analyzed with one source and two receivers operational (bistatic nodes 2-3). Due to the harsh acoustic environment, there are large numbers of false alarm contacts generated on each scan (~600 contacts formed for each FM data scan).

A simulated target was provided by an echo repeater system (E/R), which provided strong aspect-independent echoes during the runs. The E/R-originated contacts were easily identified and tagged, through an analysis of the data set. Their contact times were corrected to compensate for the E/R delay. Their SNRs were adjusted, replacing the E/R's amplification levels with values of aspect-dependent target strength (TS), obtained via the BASIS TS model. This "target injection" method modifies the data set to be more challenging, by lowering the artificially high E/R signals to more realistic,

expected, target levels. It also provides an aspect-dependent target (with the specular effect), and preserves the important environmental effects inherent in the actual data set, such as signal propagation, noise, reverberation, and clutter.

The resulting target SNRs for the TS-injected data set are shown in Fig. 20 (in green). During the run, the target's trajectory provides three specular opportunities (all on node 3) as indicated in the figure. We see that detection of specular cues could be achieved with a high threshold (HTH) setting of 30 dB, though this setting would be difficult to ascertain a priori. Observe the dropout in detections on both nodes from about 80-110 minutes, where we expect a dropout in tracker holding.

Fig. 20 also shows the maximal data series (in blue). Here, the entire measurement scan (60 seconds and 360 degrees) was used to derive the maximal data series (no segmentation was performed, though the direct blast region was ignored). The max-picked background is seen to be quite variable on node 2, between 18-28 dB, for unknown reasons. Node 3 shows a more constant maximum clutter level of about 18 dB. In either case, the max-picked background levels substantially exceed the Rayleigh case discussed in section VI. This indicates that this real ocean data background statistics to be highly non-Rayleigh. Cases where the maximal contact was target-originated can be seen when a green dot is coincident with a blue "x".

The cues identified by the algorithm are shown by the red circles. An RTH of 8 dB and an IT of 3 minutes was used, and five cue identifications were made (all on node 3). Four of these are seen to directly correspond to the three target specular events (1st, 2nd, 4th, and 5th occurring). The third identified cue is caused by a strong target-originating detection. At this point in time the target is non-specular, with a bistatic aspect angle

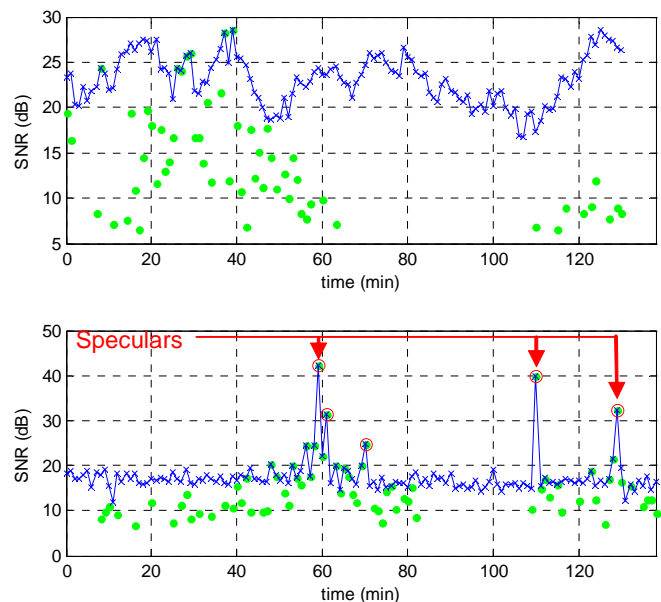


Figure 20. Data from SEABAR'07; extracted maximum values (blue); identified cues (red); target-originated contact SNRs (green); node 2 (top), node 3 (bottom).

of 100°, which corresponds to the TS enhancement of the conical tail section (seen in the BASIS model). Overall the identification method shows excellent performance finding specular occurrences in the real data.

VIII. SUMMARY AND CONCLUSIONS

An effective algorithm for automatic, data-adaptive identification of specular detections in multistatic systems has been described. The approach has been tested on two data sets, and shows good performance identifying specular detection events. This approach is more robust than using a high-detection threshold (HTH) because the parameters are tied to the expected rise in levels for specular detection events, rather than an absolute level which is difficult to know or model accurately a priori.

The identification scheme requires two parameters: the Rise Threshold and the Integration Time. Discussion and analysis has been presented on bistatic target strength, specular half-width, and bistatic aspect rate. Understanding these effects enables the proper selection of parameter values for the identification algorithm.

So far, this approach has been developed and tested independently from the SPECSweb tracking algorithm. Future work will integrate the cue identification method into the SPECSweb tracking algorithm. The envisioned approach in the tracker will designate contacts as track initiation cues if they either pass a high threshold (HTH), or, if they are identified using the data-adaptive method. In either case, designated cue's contacts will be used to initiate tracks only if they are not already associable with existing tracks.

It was observed that on occasion, the algorithm identified cues from strong target-originated contacts, when the target was not in the specular condition. Future work will attempt to also exploit these cues, by adding to the SPECSweb tracker an additional, third (back-) track initiation which does not assume a (specular) heading. This may enable tracks to be formed using strong, but non-specular target contacts. Such tracks may be confirmed earlier than specular-cued tracks, and reduce the detection latency of the SPECSweb concept.

ACKNOWLEDGEMENTS

This work was sponsored by the Office of Naval Research, 321 US.

The analysis and results for the SEABAR'07 data set was also made possible through collaboration between NATO Undersea Research Centre (NURC) and SPAWAR Systems Center Pacific.

REFERENCES

- [1] D. Grimmer and S. Coraluppi, Multistatic Active Sonar System Interoperability, Data Fusion, and Measures of Performance, NURC Technical Report NURC-FR-2006-004.
- [2] S. Coraluppi, D. Grimmer, and P. de Theije, Benchmark Evaluation of Multistatic Trackers, in Proceedings of the 9th International Conference on Information Fusion, July 2006, Florence, Italy.
- [3] D. Grimmer, Specular-Cued Multistatic Sonar Tracking on the SEABAR'07 Dataset, in Proceedings of the 12th International Conference on Information Fusion, July 2009, Seattle, Washington, U.S.A.
- [4] D. Grimmer, Multistatic Target Tracking using Specular Cue Initiation and Directed Data Retrieval, in Proceedings of the 11th International Conference on Information Fusion, July 2008, Cologne, Germany.
- [5] D. Grimmer, Reduction of False Alarm Rate in Distributed Multistatic Sonar Systems through Detection Cueing, Proceedings of the IEEE Oceans'07 Conference, June 2007, Aberdeen, Scotland.
- [6] D. Grimmer, An Effective Approach to Multistatic Tracking in Dense Clutter Environments, Proceedings of the International Symposium on Underwater Reverberation and Clutter, NATO Undersea Research Centre, La Spezia, Italy, September 2008.
- [7] D. Grimmer, S. Coraluppi, B. La Cour, C. Hempel, T. Lang, P. de Theije, P. Willet, MSTWG Multistatic Tracker Evaluation Using Simulated Scenario Data Sets, in Proceedings of the 11th International Conference on Information Fusion, July 2008, Cologne, Germany.
- [8] D. Grimmer, SPECSweb Multistatic Tracking on a Truth-Blind Simulated Scenario of the MSTWG, in Proceedings of the 12th International Conference on Information Fusion, July 2009, Seattle, Washington, U.S.A.
- [9] D. Grimmer, S. Sullivan, Sr., and J. Alsop, Modeling Specular Occurrence in Distributed Multistatic Fields, in Proceedings of the IEEE OCEANS'08 Conference, July 2008, Kobe, Japan.
- [10] S. Coraluppi and D. Grimmer, Multistatic Sonar Tracking, in Proceedings of the SPIE Conference on Signal Processing, Sensor Fusion, and Target Recognition XII, April 2003, Orlando FL, USA.
- [11] M. C. Junger, Formulation of short-wavelength bistatically scattered fields in terms of monostatic returns, in Journal of the Acoustical Society of America, 95 (6), June, 1994.
- [12] R. F. Gragg, The BASIS-3D Acoustic Target Strength Model, NRL/FR/7140--07-101052, Washington D.C., U.S.A., Naval Research Laboratory, 2002.
- [13] D. Grimmer and S. Coraluppi, Contact-Level Multistatic Sonar Data Simulator for Tracker Performance Assessment, in Proceedings of the 9th International Conference on Information Fusion, July 2006, Florence, Italy.
- [14] F. Ehlers, SEABAR'07 Cruise Report, NATO Undersea Research Center, La Spezia, Italy, 2008.